

RSC Advances



This is an *Accepted Manuscript*, which has been through the Royal Society of Chemistry peer review process and has been accepted for publication.

Accepted Manuscripts are published online shortly after acceptance, before technical editing, formatting and proof reading. Using this free service, authors can make their results available to the community, in citable form, before we publish the edited article. This *Accepted Manuscript* will be replaced by the edited, formatted and paginated article as soon as this is available.

You can find more information about *Accepted Manuscripts* in the [Information for Authors](#).

Please note that technical editing may introduce minor changes to the text and/or graphics, which may alter content. The journal's standard [Terms & Conditions](#) and the [Ethical guidelines](#) still apply. In no event shall the Royal Society of Chemistry be held responsible for any errors or omissions in this *Accepted Manuscript* or any consequences arising from the use of any information it contains.

Electrochemical performance improvement of N-doped graphene as electrode materials for supercapacitors by optimizing the functional groups[†]

Cite this: DOI: 10.1039/x0xx00000x

Received 00th January 2012,
Accepted 00th January 2012

DOI: 10.1039/x0xx00000x

www.rsc.org/

Wei Li,^{a,b,c} Hong-Yan Lü,^b Xing-Long Wu,^{*a,b} Hongyu Guan,^b Ying-Ying Wang,^{a,b} Fang Wan,^{a,b} Guang Wang,^b Li-Qun Yan,^d Hai-Ming Xie^{a,b} and Rong-Shun Wang^{*a,b}

Graphene material prepared by reducing the graphene oxide (GO, prepared by the modified Hummers method) has been considered as one of the most promising candidates of electrode materials for supercapacitors due to its mass producibility, high electrical conductivity, large specific surface area, and superior mechanical strength. However, it usually exhibits unfavorable cycling performance, mainly large capacitance fading in initial thousands of cycles, as shown but not discussed in some previous reports. In this paper, we not only find the similar phenomenon to a commercial graphene material, but also develop a very simple method to successfully enhance its electrochemical properties in terms of cycle life as well as high-rate performance, leakage current and alternating current impedance. For example, the relatively low capacitance retention of about 89.9% at the initial 1000th cycle can be increased up to 99.7% after improvement, the capacitance retention has been raised to 73% from 43% at the scan rate of 100 mV/s in cyclic voltammetry, and leakage current density has significantly more than halved (from 2.42 mA/g to 1.01 mA/g). Additionally, the reasons of improvement are also disclosed by analyzing the characterization results of X-ray photoelectron spectroscopy, electrochemical impedance spectroscopy, X-ray diffraction, Fourier transform infrared spectra and Raman spectra. It is found that, the optimization of functional groups of doped nitrogen and oxygen atoms may contribute to the improvement of cycle life and decrease of leakage current density, and the enhanced rate performance can be attributed to the increase of electrical conductivity.

1. Introduction

In recent years, considerable attention has focused on the more efficient energy storage devices with fast charge and discharge ability to relieve the pressures of increasing oil demand, depletion of non-renewable resources, and environmental pollution.¹⁻³ Among these devices, supercapacitors (SCs), also called electrochemical capacitors (ECs), represents one of the developing directions of ultrafast charge/discharge, and ultra-long cycle life.⁴⁻⁶ On the basis of energy storage mechanism, SCs are usually categorized into electrochemical double-layer capacitors (EDLCs) and pseudocapacitors.⁷ In the EDLCs, the charges are mainly stored at the electrode/electrolyte interface by the charge separation of electrode solution, which is very different from the multielectron-transfer Faradic reaction based energy storage occurring in the pseudocapacitors. Thus, the capacitance of the EDLCs is by and large proportional to the specific surface area of active electrode materials. Currently, most of the used electrode materials in commercial SCs (mainly EDLCs) are carbonaceous materials,⁸⁻¹¹ because they not only are low-cost but also could be prepared in high specific surface area larger than 2500 m²/g,¹² which could significantly increase the capacitance of SCs.

Among various kinds of carbonaceous materials, graphene, a two-dimensional carbon nanostructure with single sp²-carbon-atom thickness, has been considered as one of the most promising electrode material candidate for SCs due to its high electrical conductivity, very large specific surface area (theoretically ~2650 m²/g), and superior mechanical strength.¹³⁻¹⁷ For preparing large-scale graphene materials, modified Hummers method followed by a chemically reduced process has been proved to be the most efficient way compared with others,¹⁸ such as mechanical stripping, epitaxial growth and chemical vapor deposition. Generally, the as-obtained graphene materials prepared by this method are named as reduced graphene oxide (rGO). In the previous studies, it has been undoubtedly demonstrated that rGO usually exhibit more excellent electrochemical properties in terms of higher energy and power density compared to the traditional porous carbon materials when used as the active electrode materials for SCs if the restacking of graphene layers is effectively inhibited.^{19,20} For example, Ruoff and co-workers²¹ increased the specific surface area of graphene-derived carbon materials to 3100 m²/g by chemically activating graphene oxide, and significantly improved their gravimetric capacitance and energy density within both organic and ionic liquid electrolytes. The three-dimensional strutted graphene constructed by Wang et al²² could prevent the self-agglomeration of graphene sheets well, and

enhance the specific capacitance to as high as 250 F g^{-1} at current density of 1 A g^{-1} . By liquid electrolyte mediated method, Li and co-workers²³ optimized the ion-accessible surface of graphene materials, reduced the ion transport resistance in SCs, and hence increased the volumetric energy densities of graphene based SCs to 60 Wh L^{-1} .

In addition to energy and power densities, cycle life is another noteworthy factor for SCs evaluation, because SCs are traditionally famous for their ultra-long cycle life up to hundreds of thousands of cycles. However, we unfortunately find that most of the rGO based SCs exhibit unfavorable cycling performance, mainly large capacitance fading in the initial cycling processes, although the following cycles are relatively excellent.²⁴⁻²⁷ For instance, the capacitance fading of the initial 500 cycles of one three-dimensional rGO aerogel is as high as $\sim 10.3\%$ from $\sim 145 \text{ F g}^{-1}$ of the 1st cycle to $\sim 130 \text{ F g}^{-1}$ of the 500th cycle at the current density of 10 A g^{-1} , although that of the following thousands of cycles is only about 0.002% per cycle.²⁵ Therefore, to better realize the superiority of rGO based materials as active electrode materials for SCs, it becomes an urgent task to improve their cycle performance. Herein, we have successfully developed a simple and mass-producible method to enhance the electrochemical properties of rGO based materials as electrode materials for SCs. This method can not only improve the cycle performance, but also decrease the impedance and leakage current and hence enhance the high-rate capacitance and power density. It is noteworthy that the studied rGO is one commercial product, which promises the direct utilization of this method to commercial rGO materials and hence the development of more superior graphene products (see the photographs as shown in Figure S1) as electrode materials for SCs. Moreover, the possible reasons of improvements are also discussed based on the results of structural characterization and electrochemical measurements.

2. Experimental Section

2.1. Preparation of Thermally Stabilized rGO (TS-rGO).

Beijing Carbon Century Technology Co.,Ltd kindly provided one commercial rGO (C-rGO) product as the raw material, which were synthesized by the modified Hummers method followed by a reduction process in aqueous solution. Note that, the C-rGO is actually a nitrogen-doped rGO with high nitrogen content of about $4.5 \text{ wt}\%$ according to X-ray Photoelectron Spectroscopy (XPS) test results, because lots of carbon-nitrogen bonds would be formed in the redox processes between GO precursors and hydrazine reductant. For preparing the advanced graphene material with enhanced electrochemical properties, this nitrogen-doped C-rGO materials were placed in a quartz tube and annealed at proper temperature from 500°C to 800°C for 2 hours under high pure N_2 containing $5\% \text{ H}_2$. A large number of samples could be collected after the temperature of furnace naturally cooled to room temperature. Thereafter, the improved C-rGO materials are named as thermally stabilized rGO (abbreviated as TS-rGO) or TS-rGO(A), in which A represents the heating temperature from 500°C to 800°C .

2.2. Structural Characterization.

The morphology of all samples was firstly investigated by a scanning electron microscopy (SEM, Philips XL30, operating at 10 kV). Transmission electron microscopy (TEM) was carried out on JEOL-2100 F at 200 kV . X-ray diffraction

(XRD) patterns were recorded on a Rigaku D/max 2000 spectrometer using $\text{Cu K}\alpha$ radiation ($\lambda = 1.5406 \text{ \AA}$). Raman spectra were obtained using a Digilab FTS3500 (Bio-Rad) with a laser wavelength of 632.8 nm . X-ray photoelectron spectroscopy (XPS) was performed on the Thermo Scientific ESCALab 250Xi using 200 W monochromated $\text{Al K}\alpha$ radiation. The $500 \mu\text{m}$ X-ray spot was used for XPS analysis. The base pressure in the analysis chamber was about $3 \times 10^{-10} \text{ mbar}$. Typically the hydrocarbon C1s line at 284.8 eV from adventitious carbon is used for energy referencing. Fourier transform infrared spectra (FT-IR) were measured on Nicolet 6700. Particle size and distribution were tested on Zetasizer NanoZS (Malvern Instruments). The N_2 adsorption/desorption isotherms were measured at 77.4 K with a Micromeritics ASAP 2020 HD88 surface area analyzer.

2.3. Electrochemical Measurements.

The working electrodes were prepared by pressing a mixture of graphene-derived active materials and Teflonized acetylene black (TAB) binder at a weight ratio of 90:10 onto a 316L stainless steel mesh and then drying in vacuum at 100°C for 8h. The loading mass of active materials on the electrode substrate is ca. $6\text{-}8 \text{ mg/cm}^2$. The electrochemical properties of the prepared electrodes were carefully studied in both three-electrode and two-electrode symmetric systems in $1 \text{ mol/L H}_2\text{SO}_4$ electrolyte. While the cyclic voltammetry (CV) tests were performed in three-electrode cells using platinum electrode ($1 \times 1 \text{ cm}^2$) as the counter electrode and saturated calomel electrode (SCE) as the reference electrode, the galvanostatic cycling, leakage current test and electrochemical impedance spectroscopy (EIS) carried out in the two-electrode symmetric cells. The CVs (voltage range: $-0.2 \sim 0.95 \text{ V vs. SCE}$; scan rate: $2 \sim 100 \text{ mV s}^{-1}$) and EIS (frequency range: 100 kHz to 0.01 Hz ; amplitude: 5 mV) were measured on a PARSTAT 4000 advanced electrochemical system (Princeton Applied Research). Galvanostatic cycling tests were carried out on a LANHE 2001A system under different current densities in the voltage range of $0\text{-}1.2 \text{ V vs. SCE}$. Additionally, we also perform the galvanostatic charge/discharge tests in the electrolyte of $1 \text{ mol/L H}_2\text{SO}_4$ containing $0.1 \text{ mol/L VOSO}_4/\text{NH}_4\text{VO}_3$ to increase the energy and power densities of cells.

3. Results and Discussion

The morphological and structural variations of C-rGO in the thermally stabilized processes were firstly characterized by SEM, TEM, XRD, FT-IR, Raman and XPS technologies. As the typical SEM image shown in Figure 1a, the utilized C-rGO material is composed of uniform and wrinkled graphene layers, which is consistent with previously reported results.²⁸⁻³⁰ After thermally stabilized treatment, there is no obvious change in morphology (Figure 1b), demonstrating that heating process wouldn't cause the undesirable restacking and aggregation. Figure 1c further shows the TEM image of the TS-rGO(700) material, exhibiting obvious graphene layers with many wrinkles and twists, which is very similar with the reported TEM images of rGO materials. Because all the TS-rGO samples obtained at various heating temperatures have similar SEM images, here we only show the TS-rGO(700) one as an example. Figure 2a compares the XRD pattern of C-rGO with those of all the TS-rGO materials. It can be seen that the main

diffraction in all XRD patterns is one broad peak at around 23-25°, which corresponds to the moderately aligned graphitic

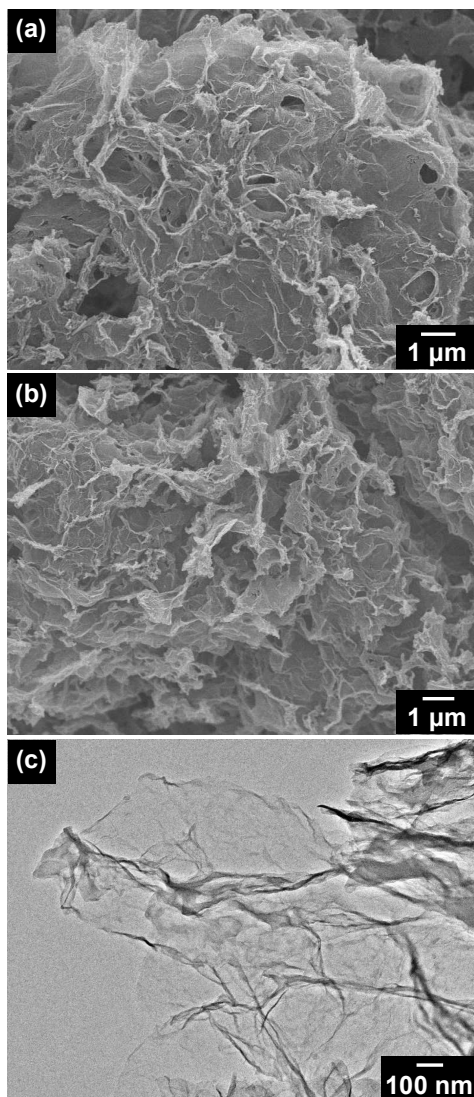


Figure 1. SEM images of (a) C-rGO and (b) TS-rGO(700), and (c) TEM image of TS-rGO(700).

arrays along the (002) direction. However, the 2θ values (25.1°) of all the thermally stabilized rGO materials are obviously larger than that (23.8°) of pristine C-rGO, indicating the reduction of interplanar distance of crystal plane (002) after heating treatment according to Bragg equation. It should be originated from the decomposition and decreases of O-/N-based functional groups in the processes of heating treatment, which has been confirmed by the following XPS and FT-IR tests.

Figure 2b shows the XPS survey spectra of all the samples. It is clearly seen that all of them are composed of three elements, i.e., carbon, oxygen and nitrogen. For the C-rGO raw material, the atomic ratio of C, O and N is about 83.89:12.07:4.04 as shown in Table 1. After thermal stabilization, the contents of O and N heteroatoms are obviously decreased, and the higher of heating temperature, the lower of the contents of doping atoms. For example, the atomic percentages of O and N are about 7.04% and 1.81% in the TS-rGO(700) materials, respectively. In addition to the variations of elemental contents and quantity of functional groups, the chemical bonding states of doping elements have also been changed in nature along with the process of thermal treatment, which will significantly affect their electrochemical properties as electrode for SCs. For example, two weak FT-IR absorption bands located at about 1734 cm^{-1} and 1655 cm^{-1} (marked as asterisks in inset of Figure S2) have disappeared after heating treatment, indicating the disappearance or reduction of the corresponding chemical bonds. The relevance between

Table 1 Elemental composition of C-rGO and TS-rGO materials calculated from XPS survey.

Samples	Atomic %		
	C	N	O
C-rGO	83.89	4.04	12.07
TS-rGO(500)	86.51	3.14	10.35
TS-rGO(600)	90.07	2.23	7.71
TS-rGO(700)	91.15	1.81	7.04
TS-rGO(800)	94.34	1.33	4.34

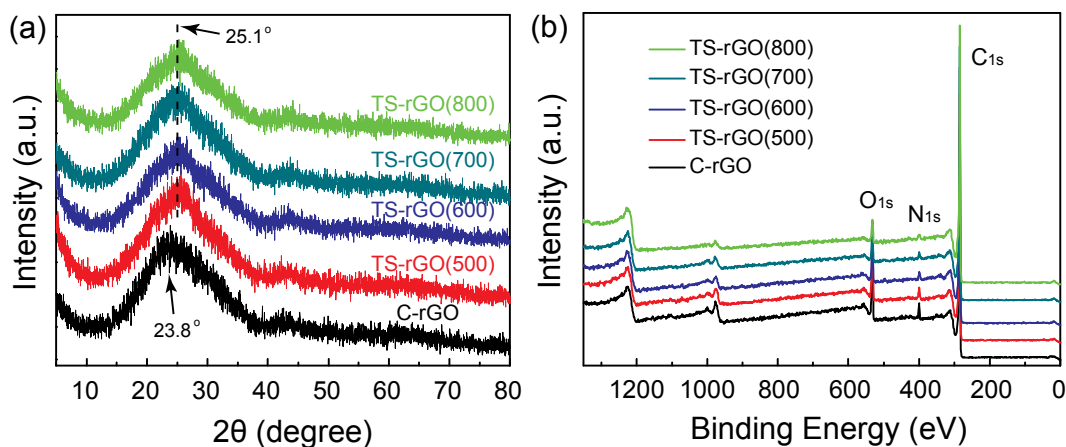


Figure 2. (a) XRD patterns and (b) XPS survey spectra of pristine C-rGO and TS-rGO materials prepared at various temperature from 500°C to 800°C.

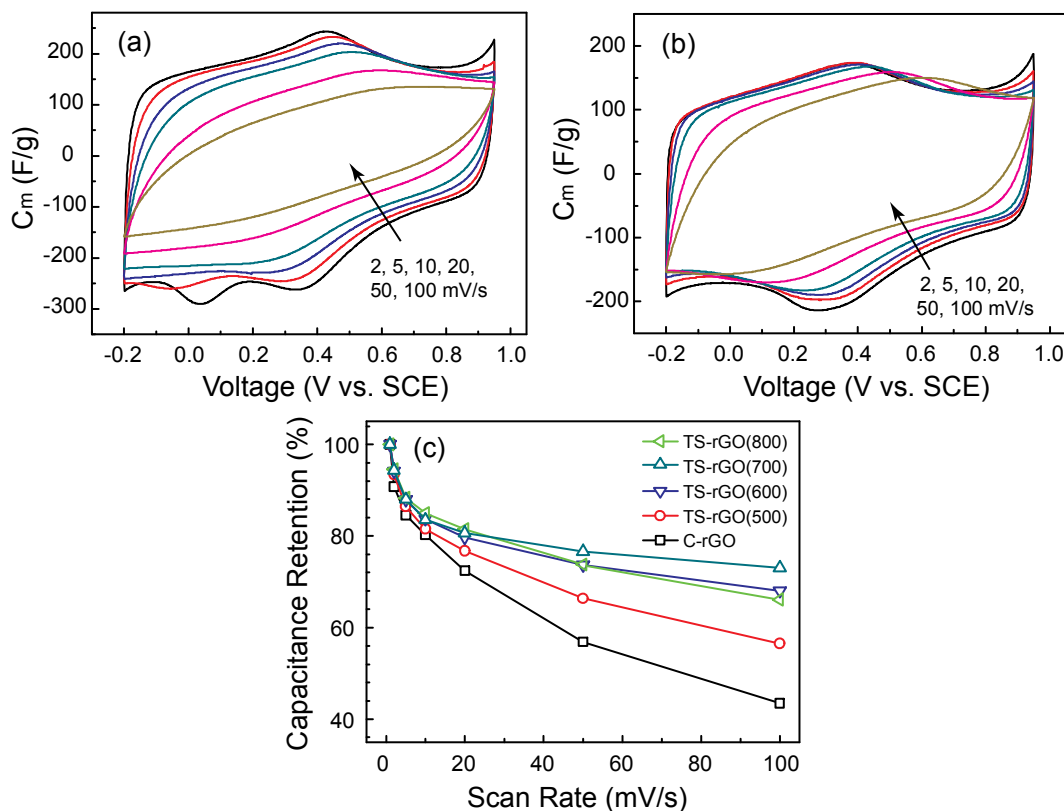
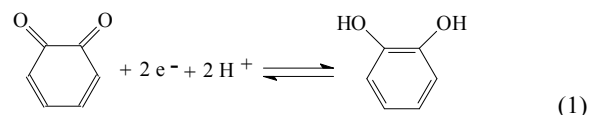


Figure 3. CV curves of (a) C-rGO and (b) TS-rGO(700) materials at various scan rate from 2 to 100 mV s⁻¹. (c) Capacity retention versus scan rate of C-rGO and TS-rGO materials.

electrochemical properties and functional groups as well as chemical bonds will be discussed in the following sections with the help of fitting of XPS profiles. Moreover, all the samples are further characterized by Raman spectra as shown in Figure S3. Two characteristic peaks located at about 1320 and 1590 cm⁻¹ correspond to the D-band and G-band of carbonaceous materials, respectively. The peak intensity ratio of D-band to G-band always keeps at around 1.4 (Table S1), demonstrating that the atomic and crystalline structures of most of carbon atoms are unchanged before and after heating treatment.

The electrochemical properties of C-rGO and all TS-rGO samples as electrode materials for SCs were evaluated in both three and two electrode systems. Figure 3a and 3b are the typical CV curves of C-rGO and TS-rGO(700) respectively. The test system used is three-electrode one, in which platinum plate in 1 × 1 cm² is counter electrode, and saturated calomel electrode (SCE) is reference electrode. As shown in Figure 3a and 3b, both exhibit nearly rectangular shapes at low scan rate of 2 mV/s. However, the CV curves of C-rGO material quickly deviate from rectangle when the scan rate is higher than 20 mV/s, while those of TS-rGO(700) material still remain almost unchanged. This implies that the thermally stabilized rGO materials will exhibit better rate performance compared to the pristine C-rGO material. Therefore, Figure 3c further compares the capacitance retention along with the increase of scan rate from 1 mV/s to 100 mV/s. All the TS-rGO materials indeed display significantly improved capacitance retention, and TS-rGO(700) material is the best one. The capacitance retention of TS-rGO(700) material is still up to 73% when the scan rate increases to 100 mV/s, while that of the pristine C-rGO material is only 43%. Below 700 °C, the capacitance retention is increased with the rise of heating temperature, because an

elevated temperature could effectively improve the electrical conductivity of products. However, when the heating temperature further rises to above 700 °C, the rate performance begins to deteriorate. As shown in Figure 3c, the capacitance retention of TS-rGO(800) material is obviously lower than that of TS-rGO(700) material when the scan rate is above 20 mV/s, although those are comparative below 20 mV/s. Those may be due to the aggravation of detrimental aggregation and restacking of graphene layers at higher heating temperature of above 700 °C, as demonstrated by the test of particle size distribution shown in Figure S5.



In addition to the rectangle-like shapes of CV curves, the pseudocapacitive peaks appeared are another interesting issues worth of attention and discussion. Firstly, there are one pair of reversible peaks at around 0.3–0.4 V vs. SCE in all CV curves of C-rGO and TS-rGO materials, which should be attributable to the oxidation/reduction of hydroquinone/quinone groups in acidic electrolyte (see equation (1)) as confirmed by Andreas and Conway.^{31, 32} The difference between potentials of anodic and cathodic peaks ($|\Delta E_{p,a-p,c}|$) in CV curves had been usually employed to evaluate the reversibility of the corresponding pseudocapacitive reaction. At low scan rate, the $|\Delta E_{p,a-p,c}|$ values of all samples before and after thermal treatment are lower than 100 mV, which is close to 59 mV and hence demonstrates their high reversibility. However, these values of C-rGO material increase sharply along with the raise of scan rate, while those of

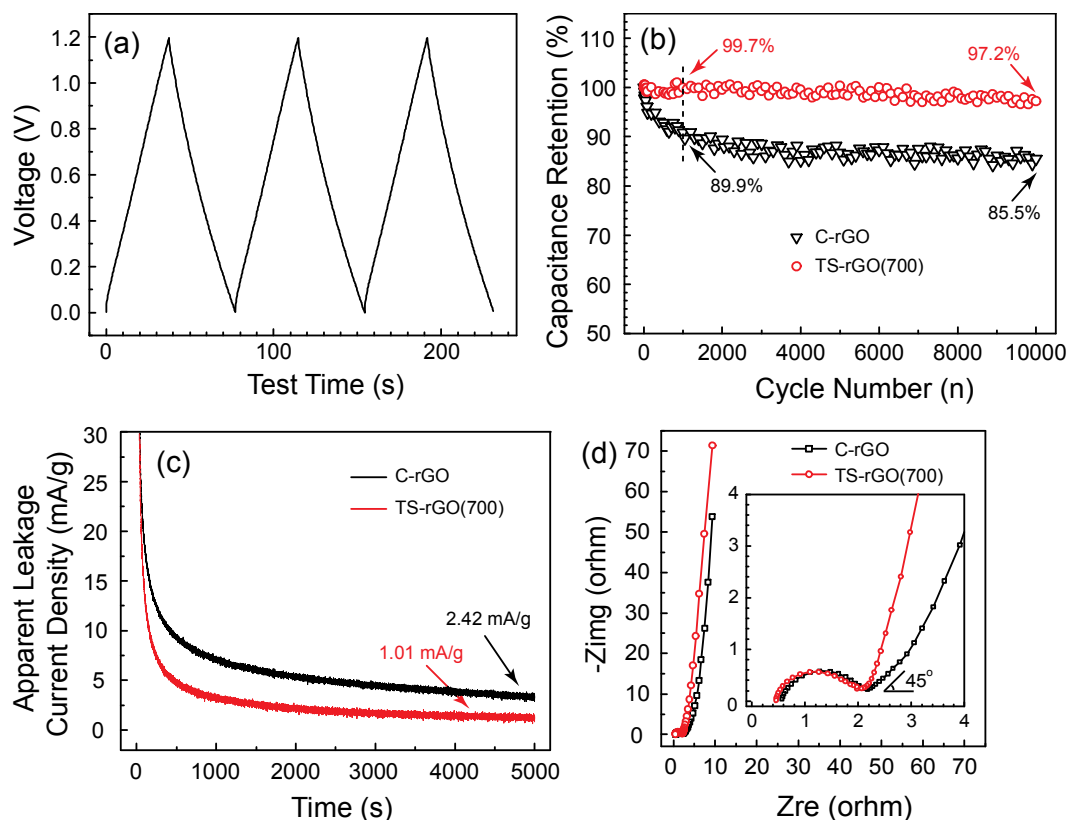


Figure 4. (a) Galvanostatic charge/discharge curve of TS-rGO(700) at current density of 2A/g. Comparison of (b) cycling performance, (c) leakage current and (d) EIS Nyquist plots for C-rGO and TS-rGO(700). Inset of (d): the partly enlarged Nyquist plots at high frequency range.

TS-rGO materials just increase slowly. Take the scan rate of 20 mV/s as an example as shown in Figure 3a and 3b, the $|\Delta E_{p,a-p,c}|$ value for TS-rGO(700) material is about 150 mV, which is much smaller than that (about 382 mV) for pristine C-rGO material. This demonstrates that the thermally stabilized treatment processes can significantly improve the reversibility of hydroquinone/quinone redox couples in the rGO based materials, especially at the scan rate above 5 mV/s, and hence further increase their high-rate capacitance (Figure 3c). Additionally, there exist extra cathodic peaks at 0-0.1 V vs. SCE in the CV curves of pristine C-rGO material compared to TS-rGO materials as shown in Figure 3a, 3b and S6. Although these pseudocapacitive peaks could increase the specific capacitance of materials, they are unfortunately unstable and irreversible. More specifically, these cathodic peaks move gradually to higher potential with lower peak current, and the corresponding anodic peaks cannot be found in the CV curves (Figure S6a). After thermal stabilization, these undesirable peaks disappear from CV curves as shown in Figure S6b, implying that the TS-rGO materials will exhibit superior electrochemical stability.

The electrochemical properties of these rGO-based materials as electrode for SCs are further studied in symmetric two-electrode cells. Here we only take the TS-rGO(700) material as the example of thermally stabilized samples to compare with pristine C-rGO material, because the TS-rGO(700) material exhibits the best high-rate performance among all the TS-rGO materials, and the variation of electrochemical properties along with heating temperature is

similar with the CV test results. Figure 4a firstly exhibits the galvanostatic charge/discharge curves of TS-rGO(700) material at 2 A/g in the voltage range of 0-1.2 V, which is symmetric and linear, indicating its superior capacitance behaviour. Figure 4b compares the cycle stability of rGO based materials before and after thermal treatment. For the pristine C-rGO material, the decay trend of specific capacitance is analogous to some previously reported results,²⁴⁻²⁷ i.e., rapid capacitance fading in the initial cycling processes followed by a relatively stable cycle life as discussed in the Section of Introduction. As shown in Figure 4b, the specific capacitance of pristine C-rGO material decreases up to 10.1% in the initial 1000 cycles, a sharp and unfavorable decay of specific capacitance, which can be effectively avoided after thermal stabilization. The capacitance retention of TS-rGO(700) is up to 99.7% in the initial 1000 cycles. Those are consistent with the CV test results (Figure S6) as discussed above. Fortunately, the specific capacitance of the pristine C-rGO material would gradually reach a relatively steady value in the following cycle process. Its capacitance decay in the following 9000 cycles is about 4.4%, which is just slightly lower than that (2.5%) of TS-rGO(700) material.

In order to give a reasonable interpretation of cycle performance improvement induced by thermal treatment, the high-resolution N1s and O1s XPS profiles of all samples are fitted as shown in Figures 5 and S7, respectively. In N-doped carbonaceous materials, the nitrogen atoms usually exist in the forms of pyridinic N (N6 at about 398.4 ± 0.2 eV), pyrrolic/pyridonic N (N5 at about 400.1 ± 0.2 eV), quaternary

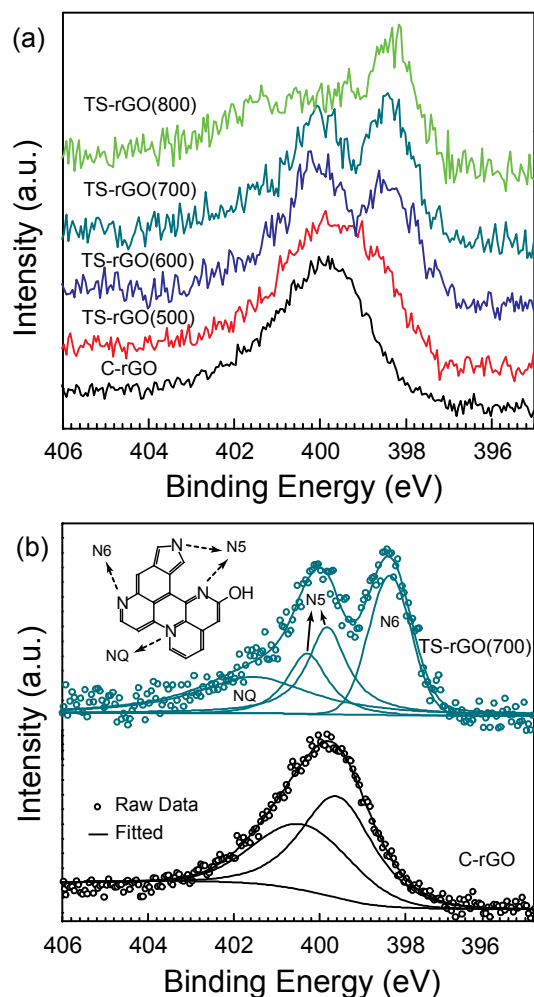


Figure 5. (a) Comparisons of N1s XPS profiles of C-rGO and TS-rGO materials prepared at various temperature from 500 °C to 800 °C. (b) The experimental and fitted N1s XPS profiles of C-rGO and TS-rGO(700). Inset of (b): a schematic illustration of N-containing groups in carbonaceous materials.

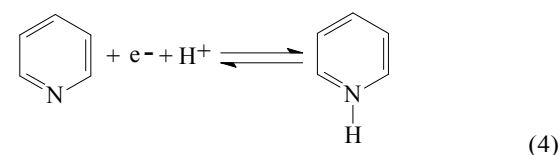
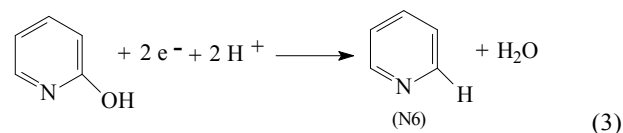
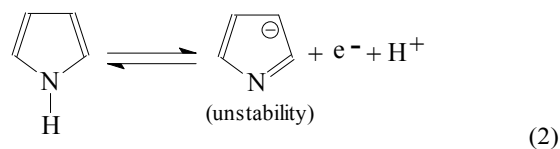
Table 2 Atomic percentages of surface nitrogen species calculated from the N1s XPS fitting.

Samples	Atomic % of nitrogen species		
	N6	N5	NQ
C-rGO	N.A.	100	N.A.
TS-rGO(500)	28.6	71.4	N.A.
TS-rGO(600)	40.7	44.3	15.0
TS-rGO(700)	43.1	30.1	26.8
TS-rGO(800)	46.3	15.4	38.3

N (NQ at about 401.4 ± 0.5 eV) and oxidized N (NX at about 402-405 eV),^{26, 27, 33} which are schematically illustrated in the inset of Figure 5b. According to the fitted results of N1s XPS profiles as shown in Figure 5 and Table 2, the doped nitrogen atoms in pristine C-rGO are almost pyrrolic/pyridonic ones. N6 and NQ atoms will appear when heating temperature rises to 500 °C and 600 °C respectively, and NX ones are always undetected at any heating temperature. Moreover, the relative percentage of both N6 and NQ are increased along with the rise of heating temperature, while the variation of N5 is on the contrary. For example, the relative contents of N6, NQ and N5

are about 43.1%, 26.8% and 30.1% (Table 2 and Figure 5b), respectively, when the heating temperature is 700 °C.

It can be rationally deduced that, the improper nitrogen functionalities existed in the pristine C-rGO material may be the main inducement of unideal cycling performance, especially huge decay of specific capacitance in the initial cycles, from the combination of test results of N1s XPS fitting, CV and galvanostatic charge/discharge cycles. The unfavorable and detrimental cathodic peaks at 0-0.1 V vs. SCE in CV curves as mentioned above (Figures 3a and S6a) should be ascribed to the electrochemical activities of nitrogen functionalities. For N5 functionalities, the possible redox reactions as illustrated in equations 2 and 3 would take place when the N-doped graphene materials tested as electrode for SCs in 1 mol/L H₂SO₄ aqueous solution.^{32, 34-36} In the processes of reactions, five-membered pyrrole will be charged and maybe gradually transformed into six-membered species due to its higher stability, while pyridonic groups charge into pyridinic ones, which will occur the reversible redox reactions as illustrated in equation 4 to contribute the pseudocapacitance³⁷. The fitting results of N1s XPS profiles demonstrate that the nitrogen functional groups in the pristine C-rGO materials are the electrochemically unstable N5 species entirely. Therefore, it exhibits unfavorable cycling performance in the initial cycles due to the irreversible changes of N5 species, and then good cycle life in the following cycles after total transformation of N5 species to stable ones. To the TS-rGO materials, the nitrogen functionalities are optimized in the thermal stabilization processes, i.e., unstable N5 structures gradually transform to stabler N6 and NQ along with the rise of heating temperature, making the irreversible cathodic peaks centred at about 0-0.1 V vs. SCE in CV curves disappear (Figures 3b and S6b) and hence improving the cycle stability of rGO based materials (Figure 4b). We also found that the higher the heating temperature implemented, the better the cycling performance exhibited. In addition to the optimization of functional groups, the change of specific surface area (SSA) in the heating processes may be responsible to the enhancement of electrochemical properties. Hence, we have further performed the test of N₂ adsorption/desorption isotherms, which are shown in Figure S4. By fitting the isotherms, it is found that the SSA values just increase slightly along with the heating temperature. In other words, the nearly constant SSA of all the products should be not one of the major factors for the improvement of electrochemical properties when used the as-prepared rGO as electrode materials for SCs.



In addition to the improvement of cycling performance, the thermal stabilization can also enhance the other electrochemical properties of rGO-based materials as electrode materials for SCs, including decrease of leakage current and increase of electrical conductivity. Leakage current is one of the another important factors to evaluate the electrochemical stability of SCs, which is related to the structures of electrode materials to a certain extent, although it is seldom mentioned in previously reported papers.³⁸ In the present work, it is excitingly found that the apparent leakage current density of symmetrical rGO-based two-electrode SCs can be significantly reduced by thermally treating the active C-rGO materials. Take the TS-rGO(700) material as an example, its apparent leakage current density (1.01 mA/g) is much lower than that (2.42 mA/g) of C-rGO material (Figure 4c), implying that the thermally stabilized r-GO materials can exhibit higher energy efficiency and lower self-discharge rate when used as electrode materials for SCs compared to pristine C-rGO material.

Furthermore, EIS spectra are further employed to compare the kinetic features of ion diffusion in C-rGO and TS-rGO(700) electrodes. As shown in Figure 4d, both are characteristic Nyquist plots with almost vertically straight line at low frequency (a typical double-layer capacitance), 45° slope at medium frequency (Warburg impedance), and semicircle at high frequency (charge transfer resistance).³⁹ The *x*-axis intercepts for C-rGO and TS-rGO(700) are 0.57 Ω and 0.46 Ω respectively, demonstrating that the internal or equivalent series resistance of TS-rGO(700) electrode is lower than that of C-rGO. It may be resulted from the higher electrical conductivity of TS-rGO(700) material compared to C-rGO material. The shorter 45° Warburg line for TS-rGO(700) further signifies the faster kinetics of ion transfer.³⁰ The radii of semicircle at high frequency for C-rGO and TS-rGO(700) electrode are almost equivalent, indicating the comparable charge transfer resistance.

Although the thermal stabilization can effectively improve the high-rate and cycling performance and decrease the leakage current density as discussed above, it unfortunately deduces the specific capacitance of the rGO based materials. And the values of specific capacitance are negatively correlated to heating temperature. According the calculated results from CV curves, the pristine C-rGO material can deliver a specific capacitance of about 210 F/g at a scan rate of 1 mV/s, which will reduce to about 187, 178, 165 and 142 F/g at the heating temperature of 500, 600, 700 and 800 °C, respectively. The similar influence laws of heating treatment on energy and power densities are also obtained from the galvanostatic charge/discharge tests of two-electrode systems. As shown in Figure 6, Ragone plots display the relationship between the energy density and power density. At relatively low power densities, the energy densities of TS-rGO(700) material are slightly lower than those of pristine C-rGO, e.g., the energy densities of TS-rGO(700) and C-rGO materials are 11.0 and 15.7 Wh/kg respectively at the power density of about 120 W/kg. Fortunately, TS-rGO(700) material will deliver higher energy densities compared to pristine C-rGO when the power density is higher than 11.5 kW/kg (Figure 6), which is consistent with the CV test results that the thermal stabilization can enhance the high-rate properties of rGO materials (Figure 3c).

For the reduced energy density in the heating processes, it can be significantly compensated by the pseudocapacitance of redox-couple-added electrolyte, as illustrated in the many reported papers.⁴⁰⁻⁴⁵ Here, 0.1 mol/L VOSO₄ and NH₄VO₃ are simultaneously added into 1 mol/L H₂SO₄ solution, forming the

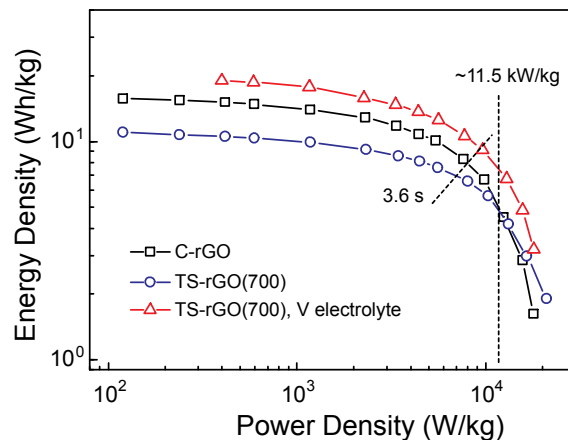


Figure 6. Comparison of Ragone plots for C-rGO and TS-rGO(700).

redox active electrolyte, which can remarkably increase the energy and power densities of TS-rGO materials to a higher level. As two Ragone plots of TS-rGO(700) materials shown in Figure 6, the energy and power densities of 0.1 mol/L VO²⁺/VO₃⁻ couple added system are about 9.35 Wh/kg and 9.5 kW/kg, respectively, both of which are higher than those (6.86 Wh/kg for energy density and 7.0 kW/kg for power density) of pristine electrolyte system, when the charge/discharge process completed in 3.6 s. This increased energy and power densities are originated from the redox-active electrolyte derived pseudocapacitance as clearly illustrated in Figure S8.

4. Conclusions

In summary, it is found that, the cycle performance of one commercial N-doped rGO material prepared from the modified Hummers method is unsatisfactory when used as electrode materials for SCs, mainly huge decay of specific capacitance in the initial cycles, which has already been displayed but not discussed in some previously reported papers. In this paper, we studied the reasons of leading to the unfavorable cycle performance and successfully developed a thermal stabilization method to enhance the cycling properties of C-rGO based materials. We found that, the doped nitrogen atoms of pyrrolic/pyridonic structures may be the main factor causing the initial decay of specific capacitance because of their instability in cycling process. After thermal stabilization treatment, these unstable functionalities transformed into more stable ones (pyridinic and quaternary nitrogen), and the corresponding cycle performance are significantly improved, e.g., the 10000th cycle capacitance retention of 700°C TS-rGO sample is up to 97.2%, which is much higher than that (85.5%) of pristine C-rGO. In addition to the enhanced cycle performance, the thermal stabilization process can also improve the high-rate capacitance, decrease the leakage current and impedance, and increase the power density. Furthermore, the unfortunately reduced energy density can be compensated by the pseudocapacitance of redox-couple-added electrolyte to higher level. This study here not only provides a simple and mass-producible method to improve the electrochemical properties of rGO based materials as electrode for supercapacitors, especially the cycle performance, but also give clear understanding of the probable reasons of improvement.

Acknowledgements

This work was supported by the National Natural Science Foundation of China (Grant Number: 51102042), the Fundamental Research Funds for the Central Universities (14QNJJ014), the Science Technology Program of Jilin Province (20140101087JC, 20150520027JH), the National High Technology Research and Development Program of China (SS2012AA110301, 2013AA110103). XL thanks the support of the International Postdoctoral Exchange Fellowship Program.

^a National & Local United Engineering Lab for Power Battery, Northeast Normal University, Changchun, Jilin 130024, P. R. China. Tel/Fax: +86-0431-85099128; E-mail: xinglong@nenu.edu.cn (XL), wangrs@nenu.edu.cn (RS).

^b Faculty of Chemistry, Northeast Normal University, Changchun, Jilin 130024, P. R. China.

^c Institute of Chemical Technology, Changchun University of Technology Changchun, Jilin 130021, P. R. China

^d Beijing Carbon Century Technology Co.,Ltd, Beijing 101400, P. R. China.

‡ These authors contributed equally to this work.

† Electronic Supplementary Information (ESI) available: [Photograph, FT-IR and Raman spectra, CV and galvanostatic charge/discharge curves, as well as O1s XPS profiles of the rGO-based samples]. See DOI: 10.1039/b000000x/

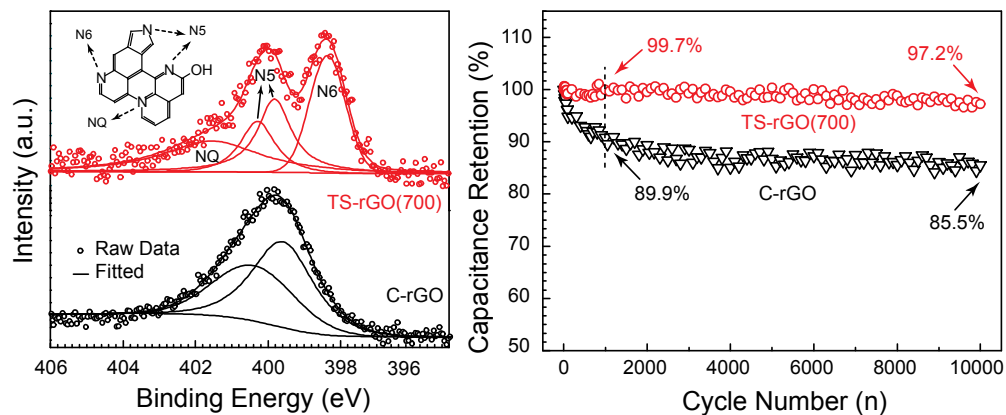
Notes and references

- P. Simon, Y. Gogotsi and B. Dunn, *Science*, 2014, **343**, 1210-1211.
- J. B. Goodenough, *Energ. Environ. Sci.*, 2014, **7**, 14-18.
- H.-G. Jung, N. Venugopal, B. Scrosati and Y.-K. Sun, *J. Power Sources*, 2013, **221**, 266-271.
- F. Beguin, V. Presser, A. Balducci and E. Frackowiak, *Adv Mater.*, 2014, **26**, 2219-2251, 2283.
- S. Lü, C. Wang and X.-T. Wang, *J. Mol. Sci.*, 2013, **29**, 290-293.
- P. Simon and Y. Gogotsi, *Acc. Chem. Res.*, 2013, **46**, 1094-1103.
- V. Augustyn, P. Simon and B. Dunn, *Energ. Environ. Sci.*, 2014, **7**, 1597-1614.
- C. Cui, W. Qian, Y. Yu, C. Kong, B. Yu, L. Xiang and F. Wei, *J. Am. Chem. Soc.*, 2014, **136**, 2256-2259.
- Y. Zhou, S. L. Candelaria, Q. Liu, Y. Huang, E. Uchaker and G. Cao, *J. Mater. Chem. A*, 2014, **2**, 8472-8482.
- R. Wang, J. Lang and X. Yan, *Sci. China Chem.*, 2014, **57**, DOI: 10.1007/s11426-11014-15123-x.
- L. Qie, W. Chen, H. Xu, X. Xiong, Y. Jiang, F. Zou, X. Hu, Y. Xin, Z. Zhang and Y. Huang, *Energ. Environ. Sci.*, 2013, **6**, 2497-2504.
- B. Liu, H. Shioyama, T. Akita and Q. Xu, *J. Am. Chem. Soc.*, 2008, **130**, 5390-5391.
- J. Liu, *Nature Nanotech.*, 2014, **9**, 739-741.
- M. D. Stoller, S. Park, Y. Zhu, J. An and R. S. Ruoff, *Nano Lett.*, 2008, **8**, 3498-3502.
- J. Zhu, D. Yang, Z. Yin, Q. Yan and H. Zhang, *Small*, 2014, **10**, 3480-3498.
- W.-Y. Tsai, R. Lin, S. Murali, L. L. Zhang, J. K. McDonough, R. S. Ruoff, P.-L. Taberna, Y. Gogotsi and P. Simon, *Nano Energy*, 2013, **2**, 403-411.
- Y. Yan, Y.-X. Yin, Y.-G. Guo and L.-J. Wan, *Adv. Energy Mater.*, 2014, DOI: 10.1002/aenm.201301584.
- A. Zurutuza and C. Marinelli, *Nature Nanotech.*, 2014, **9**, 730-734.
- H. M. Jeong, J. W. Lee, W. H. Shin, Y. J. Choi, H. J. Shin, J. K. Kang and J. W. Choi, *Nano Lett.*, 2011, **11**, 2472-2477.
- L. L. Zhang, X. Zhao, H. Ji, M. D. Stoller, L. Lai, S. Murali, S. McDonnell, B. Cleveger, R. M. Wallace and R. S. Ruoff, *Energ. Environ. Sci.*, 2012, **5**, 9618-9625.
- Y. Zhu, S. Murali, M. D. Stoller, K. J. Ganesh, W. Cai, P. J. Ferreira, A. Pirkle, R. M. Wallace, K. A. Cychoz, M. Thommes, D. Su, E. A. Stach and R. S. Ruoff, *Science*, 2011, **332**, 1537-1541.
- X. Wang, Y. Zhang, C. Zhi, X. Wang, D. Tang, Y. Xu, Q. Weng, X. Jiang, M. Mitome, D. Golberg and Y. Bando, *Nat. Commun.*, 2013, **4**, 2905.
- X. Yang, C. Cheng, Y. Wang, L. Qiu and D. Li, *Science*, 2013, **341**, 534-537.
- Y. Wang, Z. Shi, Y. Huang, Y. Ma, C. Wang, M. Chen and Y. Chen, *J. Phys. Chem. C*, 2009, **113**, 13103-13107.
- S. Ye, J. Feng and P. Wu, *ACS Appl. Mater. Interfaces*, 2013, **5**, 7122-7129.
- J. H. Lee, N. Park, B. G. Kim, D. S. Jung, K. Im, J. Hur and J. W. Choi, *ACS Nano*, 2013, **7**, 9366-9374.
- Z. Li, Z. Xu, H. Wang, J. Ding, B. Zahiri, C. M. B. Holt, X. Tan and D. Mitlin, *Energ. Environ. Sci.*, 2014, **7**, 1708-1718.
- X. Zhou, Y.-X. Yin, L.-J. Wan and Y.-G. Guo, *Adv. Energy Mater.*, 2012, **2**, 1086-1090.
- K. Parvez, Z.-S. Wu, R. Li, X. Liu, R. Graf, X. Feng and K. Müllen, *J. Am. Chem. Soc.*, 2014, **136**, 6083-6091.
- N. Xiao, H. Tan, J. Zhu, L. Tan, X. Rui, X. Dong and Q. Yan, *ACS Appl. Mater. Interfaces*, 2013, **5**, 9656-9662.
- H. A. Andreas and B. E. Conway, *Electrochim. Acta*, 2006, **51**, 6510-6520.
- Y.-H. Lee, K.-H. Chang and C.-C. Hu, *J. Power Sources*, 2013, **227**, 300-308.
- J. Machnikowski, B. Grzyb, J. V. Weber, E. Frackowiak, J. N. Rouzaud and F. Béguin, *Electrochim. Acta*, 2004, **49**, 423-432.
- E. Frackowiak, G. Lota, J. Machnikowski, C. Vix-Guterl and F. Béguin, *Electrochim. Acta*, 2006, **51**, 2209-2214.
- G. Lota, K. Lota and E. Frackowiak, *Electrochem. Commun.*, 2007, **9**, 1828-1832.
- E. Frackowiak, *Phys. Chem. Chem. Phys.*, 2007, **9**, 1774-1785.
- D.-W. Wang, F. Li, L.-C. Yin, X. Lu, Z.-G. Chen, I. R. Gentle, G. Q. Lu and H.-M. Cheng, *Chem. Eur. J.*, 2012, **18**, 5345-5351.
- X.-G. Zhuang, Y.-S. Yang, D.-P. Yang, Y.-J. Ji and Z.-Y. Tang, *Battery*, 2003, **33**, 199-202.
- X.-L. Wu, W. Wang, Y.-G. Guo and L.-J. Wan, *J. Nanosci. Nanotech.*, 2011, **11**, 1897-1904.
- E. Frackowiak, K. Fic, M. Meller and G. Lota, *ChemSusChem*, 2012, **5**, 1181-1185.
- L. Chen, H. Bai, Z. Huang and L. Li, *Energ. Environ. Sci.*, 2014, **7**, 1750-1759.
- C. Zhao, W. Zheng, X. Wang, H. Zhang, X. Cui and H. Wang, *Sci. Rep.*, 2013, **3**, 2986.

43. S. T. Senthilkumar, R. K. Selvan, Y. S. Lee and J. S. Melo, *J. Mater. Chem. A*, 2013, **1**, 1086-1095.
44. S. T. Senthilkumar, R. K. Selvan, N. Ponpandian, J. S. Melo and Y. S. Lee, *J. Mater. Chem. A*, 2013, **1**, 7913-7919.
45. H. Yu, J. Wu, L. Fan, Y. Lin, S. Chen, Y. Chen, J. Wang, M. Huang, J. Lin, Z. Lan and Y. Huang, *Sci. China Chem.*, 2012, **55**, 1319-1324.

Table of Contents

TOC figure:



TOC text:

The electrochemical properties of doped graphene as electrode materials for supercapacitors can be significantly enhanced by optimizing the surface nitrogen functional groups.